Mon. Not. R. Astron. Soc. **000**, 000–000 (0000) Printed 1 February 2008 (MN LATEX style file v1.4)

Soft versus Hard X–Ray Emission in AGN: Partial Covering and Warm plus Cold Absorber Models

M.T. Ceballos[1,2] & X. Barcons[1]

[1] *Instituto de Física de Cantabria (Consejo Superior de Investigaciones Científicas - Universidad de Cantabria), 39005 Santander, Spain*

[2] *Departamento de Física Moderna, Universidad de Cantabria, 39005 Santander, Spain*

1 February 2008

ABSTRACT

We analyse the *ROSAT* PSPC hardness ratio and the 0.5-2 keV to 2-10 keV flux ratio of 65 Active Galactic Nuclei (AGN) for which there are both *ROSAT* archival observations available and 2-10 keV fluxes, mostly from the HEAO-1 MC-LASS survey. We conclude that the simplest spectral model for the AGN that can accommodate the variety of X-ray colours obtained is a standard power law (with energy spectral index $\alpha \sim 0.9$) plus a ~ 0.1 keV black body both partially absorbed. In our sample, type 1 AGN require an absorbing column around $10^{22}\,\mathrm{cm}^{-2}$ with covering fractions between 20 and 100%, while type 2 AGN display larger columns and $\sim 100\%$ coverage. This simple model also provides a good link between soft and hard AGN X-ray luminosity functions and source counts. We also consider a warm absorber as an alternative model to partial covering and find that the the presence of gas in two phases (ionized and neutral) is required.

Key words: X–rays: general - X-rays: galaxies - galaxies: active - galaxies: nuclei

1 INTRODUCTION

Comparing the information obtained through the analyses of AGN data in different X-ray energy bands appears to be a difficult task which leads in some cases to striking results. For example, 2-10 keV X-ray source counts (which are dominated by AGN) obtained by the *Ginga* fluctuation analyses (Warwick & Butcher 1992) are clearly above the number counts obtained from the *Einstein Observatory Medium Sensitivity Survey* (EMSS) in the 0.3-3.5 keV band (Gioia et al. 1990) if a power law spectrum with energy spectral index $\alpha \gtrsim 0.7$ and negligible photoelectric absorption are assumed. Several explanations have been proposed to bring these results into consistency. Warwick & Butcher (1992) were able to fit the spectrum of the fluctuations in the 2-10 keV band (which should be close to the median X-ray spectrum of a source at the level where there is one source per *Ginga* LAC beam $\sim 5\times10^{-13}\,\mathrm{erg\,cm^{-2}\,s^{-1}}$) to a power law with an energy spectral index $\alpha \approx 0.8$ with no evidence for photoelectric absorption (the derived upper limit is $N_H \lesssim 3\times10^{21}\mathrm{cm}^{-2}$, Stewart 1992). In order to have a 2-10 keV to 0.3-3.5 keV flux ratio of about 2 (which is what is needed in order to reconcile source counts in both energy bands) a photoelectric absorption larger than the above upper limit is required. In this case, the contribution of clusters of galaxies, having a much softer spectrum will compensate the AGN photoelectric absorption in the spectrum of the fluctuations (Barcons 1993). If photoelectric absorption were ignored, an energy spectral index $\alpha \sim 0.4$, much flatter than the typical index for any class of source (and this indeed includes AGN) at that flux level, would be required. Therefore, absorption in AGN appears to be a necessity to solve the soft/hard X-ray source counts discrepancies.

On the other hand, soft X-ray selected AGN actually exhibit low-energy excesses over the average power law (Maccacaro et al. 1988, Turner and Pounds 1989, Hasinger 1992). Franceschini et al. (1993) proposed a scenario to account for these facts: the existence of two different populations, the soft X–ray sources, with steep spectrum and high evolution rates and the hard X-ray sources, with a weak cosmological evolution and strong self-absorption. Recent models for the origin of the X-ray background (Madau, Ghisellini & Fabian 1994, Comastri et al 1995) based on the AGN unified scheme (Antonucci & Miller 1985, Antonucci 1993), rather suggest that there is a continuity between these two populations.

We analyse a sample of AGN for which there are 2-10 keV fluxes (mostly coming from the HEAO-1 MC-LASS survey, Wood et al 1984) and archival *Rosat* PSPC observations. By analysing the PSPC hardness ratios versus 0.5-2 keV to 2-10 keV flux ratio, we conclude that the simplest spectral model that can accommodate the whole sample is a power law plus a blackbody both partially absorbed.

Furthermore the model we propose is able to bring into consistency the source counts as well as the AGN luminosity functions in both bands. Our comparison is relevant only to local ($z < 0.2$) AGN and its extension to higher redshifts would require more data.

We also consider an alternative to this partial covering scenario which can account for the spectra of AGN as well as for the soft excess observed: a full obscuration of the X–ray continuum by partly ionized gas (see Netzer 1993 and references therein). However unless some neutral absorbing material is also present the spectra are invariably too soft.

In section 2 we describe the sample, present the broad-band hardness ratio versus flux ratio relation, and introduce the simplest model also able to accommodate the wide range of parameter space occupied by these sources. The warm absorber model is also introduced in this section as an alternative model to describe the spread in the observed parameters. In section 3 we show that a partial covering model is able to bring soft and hard X-ray AGN luminosity functions and source counts into agreement. We summarize the results and present some conclusions in section 4.

2 BROAD BAND HARDNESS RATIOS

2.1 The sample

In order to study the Broad Band X-ray colours, we constructed a local (z<0.2) AGN sample, in such a way that K-corrections or evolutionary effects do not come into play. We tried to build the largest sample for which there is a 2-10 keV flux measurement and *Rosat* PSPC information contained in the WGACAT point source catalogue in the public archive at *HEASARC*. The resulting sample is listed in Table 1.

Most of the objects come from the LMA sample described by Grossan (1992), which is the AGN sample of the HEAO-1 MC-LASS, from which we take the 2-10 keV fluxes. Other AGN with 2-10 keV fluxes measured either by *Ginga* (19 sources, Awaki 1992, Nandra and Pounds 1994, Turner et al 1992b) or *EXOSAT* (5 sources, Turner & Pounds 1989) have also been included. However our conclusions remain unaffected if these low luminosity objects (the *Ginga* and *EXOSAT* ones) are removed. From the LMA sample we had to eliminate two sources known to be contaminated by another nearby source: III Zw 2 (Tagliaferri et al 1988) and 3A0057-383 (Giommi et al 1989, George et al 1995). From the EXOSAT sub-sample we also eliminate 3C445 which is close to the cluster of galaxies A2440 which can contaminate its 2–10 keV flux. The WGACAT point source catalogue provides the counts collected by the PSPC in the soft (11-39) PI channels and in the hard (40-200) PI channels. The 0.5-2 keV fluxes have been obtained from these data, under the assumption of an energy spectral index of $\alpha = 0.9$ and Galactic photoelectric absorption (also given in the WGACAT point source catalogue), although our conclusions remain unaffected if other model spectra are assumed.

Indeed, the 2-10 keV and *Rosat* PSPC observations are not simultaneous and therefore variability could be relevant for each source individually. However, we do not intend here to derive specific spectral properties for each source, but we rather regard the AGN sample as an ensemble and therefore no systematic variations in the X-ray colours are expected from the variability. But even for individual sources, a factor of 2 variation in the flux ratios (see below) will not affect our conclusions.

2.2 Hardness ratios.

We defined a source hardness ratio in the soft band as:

$$HR = \frac{H - S}{H + S} \quad (1)$$

S being the number of counts in ROSAT PI channels 11-39 (0.1-0.4 keV) and H the number of counts in channels 40-200 (0.4-2.0 keV).

In Figure 1 we plot the PSPC hardness ratio (corrected for Galactic absorption) versus flux ratio, defined as the ratio between the soft (0.5-2 keV) band flux and the hard band flux (2-10 keV), for the sample described above. The Galactic correction is strongly dependent on the model assumed so we used the spectral model described below in order to be self-consistent. Maybe the most striking feature of this plot is the large spread of the AGN population. That indeed implies that there is no universal AGN spectrum.

In order to explain this colour-colour diagram exhibited by the sources we carried out some simulations with XSPEC, assuming model spectra for the sources and folding them through the ROSAT PSPC response matrix to obtain the counts in each channel (from which we compute S and H) as well as the fluxes in the soft (0.5-2 keV) and hard (2-10 keV) energy bands.

The simplest model for the AGN spectrum, an unabsorbed power law, turns out to be unable to reproduce the scatter observed in the hardness ratios even if the energy spectral index is allowed to vary. This is clearly shown in figure 2 where we show the expected position in the X-ray colour diagram by this model for a couple of typical energy spectral indices.

The next step, is to assume some intrinsic photoelectric absorption for the AGN. The solid line in Figure 2 is obtained by varying the column density for an $\alpha = 0.9$ standard power law, from the Galactic value to $\sim 10^{24}\,\mathrm{cm}^{-2}$. With this model, a wider range of hardness ratios would be covered. Moreover higher flux ratios (F(0.5–2)/F(2–10)$\geq$0.6) could be obtained if steeper power laws were taken into account. Yet moving the energy index within a reasonable range ($0.7 \lesssim \alpha \lesssim 1.0$) results in the flux ratio changing from ~ 0.5 to ~ 1, which does not explain the ratios observed for the sources in figure 1, some of which are greater than one and others much smaller than 0.5.

Therefore the dispersion observed in the colour–colour plot seems to require a more complex spectrum. To solve the problem of high flux ratios we added a third component to the spectral model just to increase the soft emission. We modified the previous spectrum with a blackbody component with temperature $kT = 0.1$ keV which is similar to temperatures fitted to the soft excess emission of some AGN (Kaastra, Kunieda & Awaki 1991, Turner et al 1992a, Matsuoka 1994 and references therein). The result is represented in figure 2 as a dashed line which was produced by assuming $\alpha = 0.9$ and by changing the column density of absorbing gas from Galactic to $10^{24}\mathrm{cm}^{-2}$.

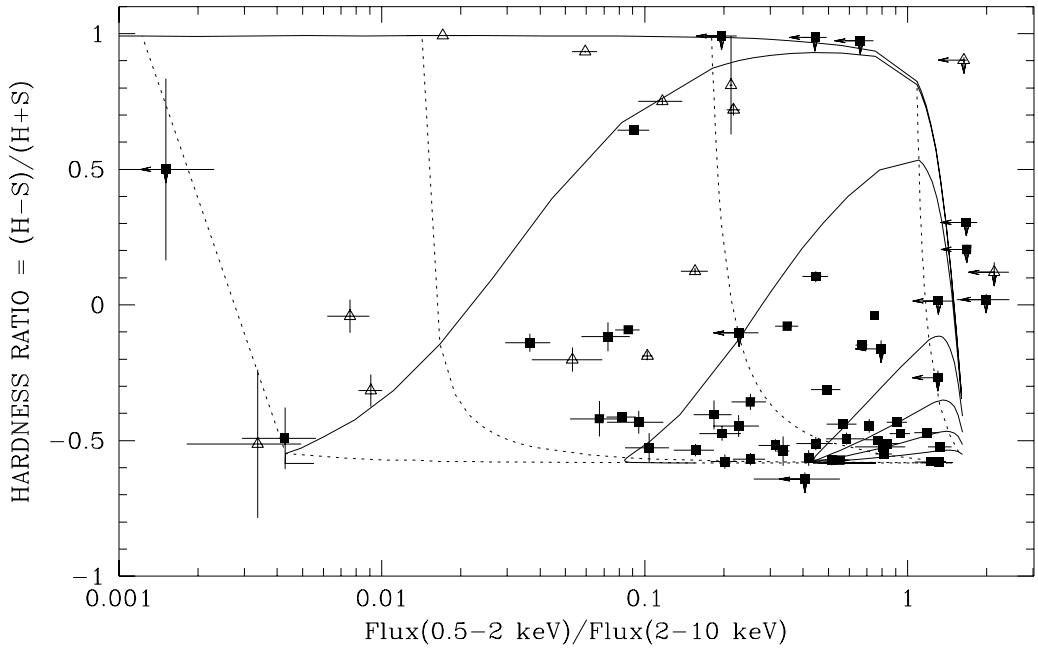

Figure 1. ROSAT PSPC hardness ratio (corrected for Galactic absorption according to the spectral model explained in 2.2) versus flux ratio. H and S are the counts in the PI channels 40-200 and 11-39 respectively. The individual points represent the sources in the sample, Seyfert 1 or QSO (filled squares) and Seyfert 2 (open triangles). Along each solid line the covering factor in the simulation is kept constant whereas the column density parameter changes from $10^{20}\mathrm{cm}^{-2}$ to $3\times10^{23}\mathrm{cm}^{-2}$ from right to left. The values assumed for the covering factor are f_{cov}= 0.20 (lower solid line), 0.40, 0.60, 0.80, 0.97, 0.999, 1.00 (uppermost curve). The dotted lines have constant column density values, $N_H = 10^{21}$ (dotted line on the right), 10^{22}, 5×10^{22}, 10^{23} (dotted line on the left) and the covering factor ranges from 0.2 to 1.0 from bottom to top along the line.

By comparing the models above (Figure 2) and the data (Figure 1), we still see that for an absorbed spectrum, the PSPC hardness ratios are often much smaller than would be predicted from the 0.5-2 keV to 2-10 keV flux ratio. The simplest model that can modify this is a partial covering model, where the absorbing gas only covers a fraction f_{cov} of the source towards the observer. This 'minimal' spectral model is then

$$F(E) = (A_1 \frac{E^3}{e^{E/kT}-1} + A_2\, E^{-\alpha}) \qquad (2)$$

$$[1 - f_{cov} + f_{cov}\, e^{-\sigma(E)\, N_H}]$$

where $\sigma(E)$ is the absorption cross-section. A_1 and A_2 give relative weights to the power law and the black body.

In order to interpret the data in figure 1, we kept the power law energy index $\alpha = 0.9$ constant, the blackbody temperature $kT = 0.1$ keV and its relative contribution (50% of the power law at 1 keV) constant and repeated the simulations for different values of the column density and the covering factor parameters. The result of the simulations is presented in figure 1 with solid and dotted lines. Each solid line corresponds to a different covering factor from 20% (bottom) to 100% (top) and is generated with different values for the column density that grow from right to left along the curve from 10^{20}to3×10^{23} cm^{-2}. Each dotted line is drawn keeping constant the column density whereas the covering factor grows from bottom to top. The N_H value ranges from 10^{21} cm^{-2} (first dotted line on the right) to 3×10^{23} cm^{-2} (dotted line on the left).

We also based on this model to correct the hardness ratios for the effects of Galactic absorption due to its simplicity although as it will be shown at the end of the section there is an alternative model able to describe the behaviour of the broad band X–ray colours. In order to do this correction we defined a model spectrum just as the one presented above: a power law (with the energy index fixed to 0.9), a black body (temperature of 0.1 keV and relative contribution of 50% also fixed) both partially absorbed by an intrinsic column density plus an extra absorption representing the effect of the Galaxy. We folded it through the ROSAT response matrix and repeated the simulations for a grid of values of the intrinsic column density and the covering factor and for the values of the Galactic absorption presented by the sources in the sample. A plot similar to that in Figure 1 was then obtained for each source (i.e, for each Galactic column density). The estimated values of the spectral parameters involved (partial covering factor and intrinsic column density) were obtained just doing a bilinear interpolation. With these "true" parameters we folded again the spectrum for each source so as to get the corrected Hardness ratio.

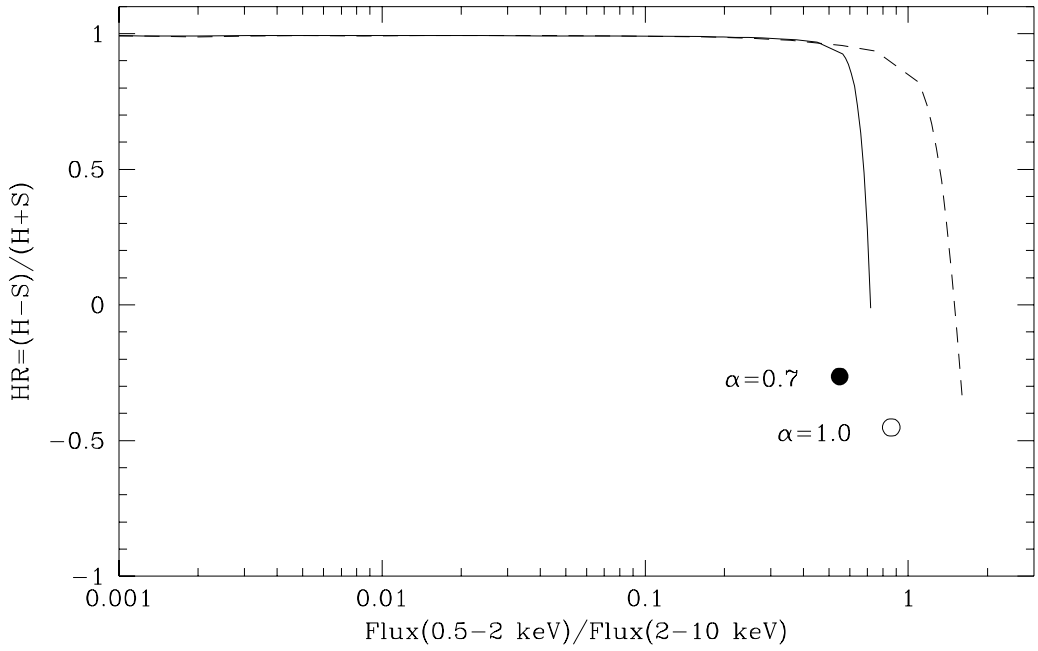

Figure 2. Simulated hardness ratio versus flux ratio for different spectral models. Filled circle: power law with $\alpha = 0.7$. Hollow circle: power law with $\alpha = 1.0$. Solid line: absorbed power law with $\alpha = 0.9$ and column density ranging from 10^{20} to $10^{24}\,\mathrm{cm}^{-2}$ from right to left along the line. Dashed line: absorbed power law with $\alpha = 0.9$, blackbody temperature $kT = 0.1$ keV and contribution of 50% of the power law at 1 keV and column density ranging from 10^{20} to $10^{24}\,\mathrm{cm}^{-2}$ from right to left along the line.

Some of the sources (appearing as arrows in the plot) were not corrected since they fall off this simple model with the parameters fixed above requiring a model with slightly different values of the power law energy index and/or black body temperature and relative contribution. Thus these sources are shown as upper limits since the Galactic absorption tends to soften the hardness ratio and to lower the flux ratio.

Concerning the AGN type (type 1 and type 2) it appears that each class requires different parameters. While the Seyfert 1 and QSO show a greater dispersion in the parameters, Seyfert 2 tend to accumulate around a covering factor of the order of 100% and/or high column densities (with the exception of NGC 1068) in agreement with observations of individual objects (Awaki 1992). For the majority of the type 1 AGNs in our sample we infer an absorbing column $\approx 10^{22}\,\mathrm{cm}^{-2}$ and a covering fraction f_{cov} between 80% and 100%. The range over which this last parameter varies is particularly sensitive to the assumed blackbody temperature (i.e., at lower blackbody temperatures the unabsorbed spectrum is softer and therefore more coverage is required), but in any case there is always an important fraction of the type 1 AGN which require partial coverage.

If we restrict ourselves to the LMA sources (the LMA sample is flux limited at 5 keV), the average covering fraction for the type 1 AGN is $0.818^{+0.031}_{-0.036}$ while for the type 2 AGN the average covering fraction is 0.9985 ± 0.0007. It has to be said, however, that although this subsample is selected in hard X-rays and therefore there should not be strong biases towards low covering factors, we only use those AGN for which there is information in the WGACAT point source catalogue. This might introduce a slight bias towards low covering factors, but we do not expect it to be too strong, except for the objects with the largest absorbing columns (essentially the Seyfert 2s). Indeed, for soft X-ray selected samples of AGN, the average covering factor is expected to be larger.

We tried to find a similar description of the data in terms of a warm absorber model (Turner et al 1991, Netzer 1993 and references therein, Reynolds and Fabian 1995). We used the photoionization code XSTAR (Kallman and McCray 1982, Kallman and Krolik 1993) to reproduce the conditions of a thin shell of gas ionized by a primary continuum of energy index 0.9 and luminosity $L = 4 \times 10^{43}$erg/s. The gas density was fixed to $n = 10^{9}\mathrm{cm}^{-3}$ and XSTAR was run for different ionization parameters ranging from $\xi = 20$ to $\xi = 40$ where $\xi \equiv L/(nR^2)$. We selected the XSTAR output to give the fractional abundance of the ions in the gas (relative to the total hydrogen abundance), their K-edge energy and their photoionization cross sections. With these values we constructed a spectrum model for each gas state (defined by a ionization parameter and a column density of neutral hydrogen N_H). This spectrum was folded through the ROSAT PSPC response matrix in XSPEC to calculate the hardness ratios just as it was done with the partial covering model. The spectrum consisted of a power law of energy

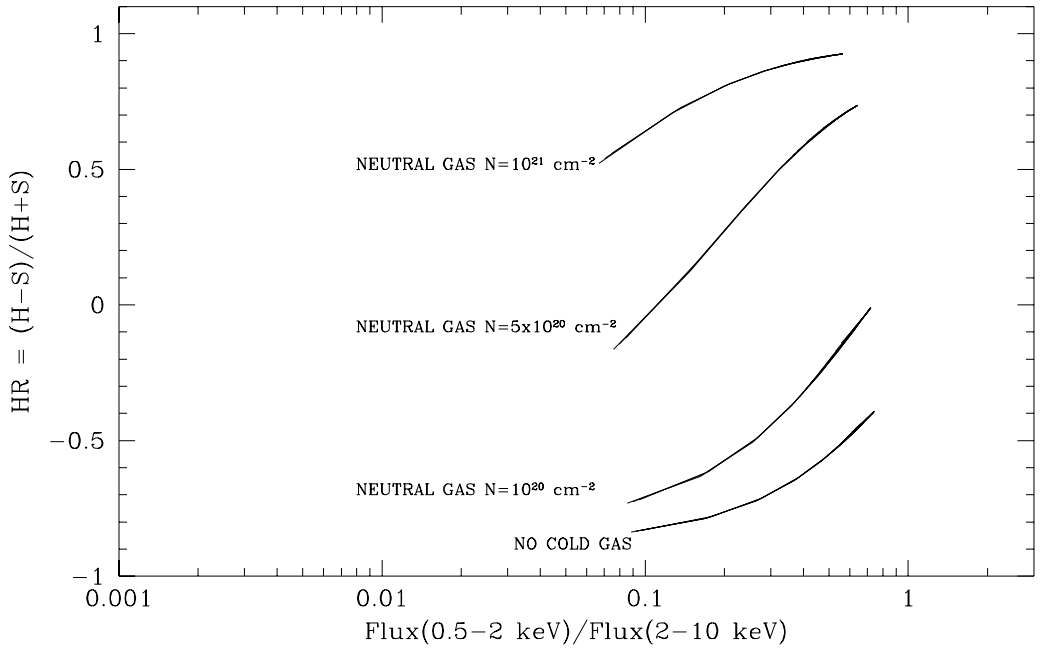

Figure 3. Simulated hardness ratios versus flux ratios for a warm absorber model (see text). The three uppermost curves correspond to neutral gas added to the warm component.

index $\alpha = 0.9$ and an absorption edge for every ion with significant depth at the threshold ($\tau \geq 0.01$) for a given N_H. The values of the N_H ranged from 10^{19} to10^{22} cm^{-2}). The resulting hardness ratio versus flux ratio relation is showed in figure 3 as a solid line.

As it is shown in this figure the variety of X–ray colours cannot be accounted for only with this model of ionized gas. Thus, in order to obtain "harder" colours we added a neutral gas component to the spectra defined above. The results for three equivalent neutral hydrogen column densities in addition to the warm absorber component are presented in figure 3.

We show that in order to reproduce the variety of broad band X–ray colours observed in the sample a new component of neutral gas must be added to the partly ionized gas.

3 LUMINOSITY FUNCTIONS

We derived the local luminosity function in the hard band (2-10 keV) so as to compare it with the luminosity function coming from the soft band (Boyle et al 1994, Maccacaro et al 1991). This can be used to test whether the simple model presented in this paper predicts a correct link between soft and hard X-ray energies.

The local luminosity function in the 2-10 keV band is derived from the whole Grossan (1992) LMA sample (irrespective on whether or not *Rosat* observations exist) restricted to those sources with redshifts lower than 0.2 and turning to the technique of maximum likelihood analysis used by Marshall et al. (1983). In his analysis of the luminosity function for the whole sample, Grossan showed that a single power law fit was only good as an approximation but that it was unacceptable for the full range of luminosities since the luminosity function steepens at high luminosities. Therefore we decided to use a broken power law form to fit the local hard band luminosity:

$$\Phi(L_{44}) = \begin{cases} K_1\, L_{44}^{-\gamma_1} & \text{if } L_{44} \leq L_{br} \\ K_2\, L_{44}^{-\gamma_2} & \text{if } L_{44} > L_{br} \end{cases} \tag{3}$$

where K_1 is the normalization of the luminosity function and γ_1 and γ_2 are the faint and the bright end slopes respectively. The constant K_2 is related to the normalization value through the 'break' luminosity, L_{br}:

$$K_2 = K_1\, L_{br}^{\gamma_2 - \gamma 1} \tag{4}$$

L_{44} is the 2-10 keV X-ray luminosity function expressed in units of 10^{44} erg/s.

In spite of the fact that this sample is reduced to almost local sources ($z \leq 0.2$) the luminosity of the sources was deevolved to $z = 0$ using a power law evolution form (pure luminosity evolution):

$$L_{44} = L_{44}(z)\,(1+z)^{-\beta} \tag{5}$$

with $\beta = 2.6$ (Maccacaro et al 1991).

The best-fit values from the maximum likelihood analysis are $\gamma_1 = 2.11^{+0.08}_{-0.09}$, $\gamma_2 = 3.27^{+0.41}_{-0.25}$, $\log(L_{br}) = 44.51^{+0.11}_{-0.10}$ and $K_1 = 6.50 \times 10^{-7}$ Mpc^{-3} $(10^{44}$ erg/s$)^{-1}$. We tested the goodness of fit of the model fit to the data applying a KS statistic a high level of acceptability.

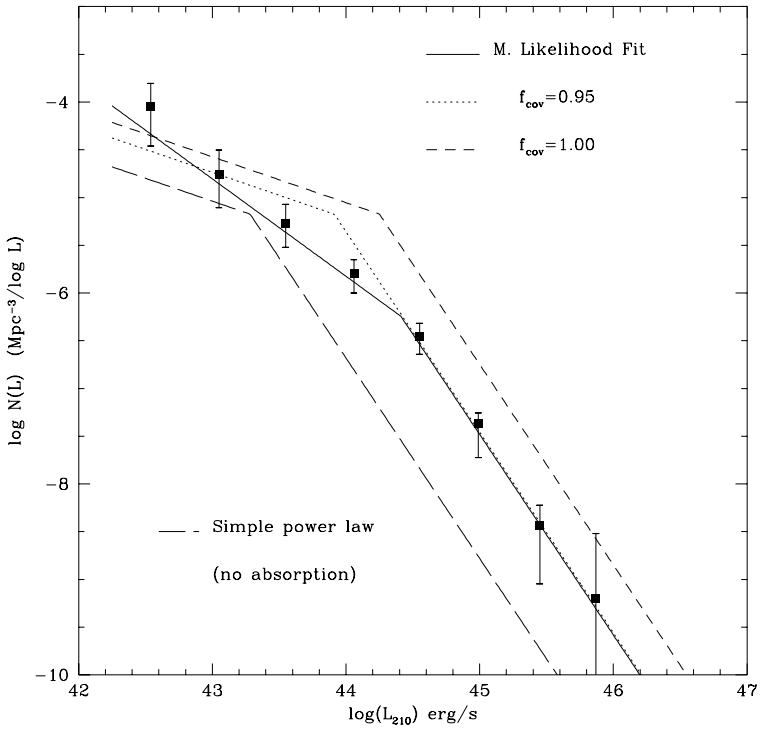

Figure 4. 2–10 keV local ($z < 0.2$) Luminosity Function. The solid line represents the maximum likelihood fit to the hard band sample. The Maccacaro et al. (1991) soft luminosity function was moved into this hard band assuming a power law energy index $\alpha = 0.9$, a blackbody temperature and contribution of $kT = 0.1$ keV and 50% at 1 keV respectively, $N_H = 10^{22}\,\mathrm{cm}^{-2}$ and two different covering factors: 0.95(long-dashed line) and 1.0 (dot-dashed line). The points with the error bars reproduce the nonparametric fit to the sample with the $1/V_a$ method.

The comparison between the two luminosity functions is shown in Figure 4, which displays the binned 2-10 keV luminosity function together with the maximum likelihood fit and some models. As usual, we assume a broken power law for the soft X-ray luminosity function, and the specific parameters are taken from the *Einstein Observatory* Extended Medium Sensitivity Survey (Maccacaro et al 1991). We prefer this survey to the Boyle et al (1994) one as a comparison with our 2-10 keV sample, because the Boyle et al (1994) sample contains virtually no objects at redshifts $z < 0.4$ and therefore the local luminosity function derived in that paper is much affected by the specific evolution models. The soft-to-hard band conversion has been done with a set of 'averaged' values for the parameters of the partial covering spectral model: $\alpha = 0.9$, $kT = 0.1$ keV, a blackbody contribution $\sim 50\%$ at 1 keV, $N_H = 10^{22}\,\mathrm{cm}^2$ and different covering factors. Again, we must stress here that we use this particular model due to its simplicity. The same conclusions should be obtained through the neutral plus ionized gas model since both models are able to reproduce the dispersion observed in the X–ray colours versus flux ratios relation. The points with the error bars in the plot correspond to a nonparametric representation of the 2 - 10 keV luminosity function obtained with the $1/V_a$ method developed by Avni and Bachall (1980).

As it can be seen from Figure 4 a perfect agreement is rather difficult to obtain due to the large number of variable parameters involved in the description of the sources spectrum, specially at and below the break. Once we fixed some parameters as blackbody temperature and its fractional contribution, power law energy index and absorption column density, it can be seen that very good agreement between both functions at luminosities $> 10^{44}\,\mathrm{erg\,s}^{-1}$ is reached for a covering factor ~ 0.95. The fit is poorer for luminosities lower than $L_{2-10} \sim 10^{44}\,\mathrm{erg\,s}^{-1}$ because it is not possible to introduce the dispersion observed in the values of some parameters as the column density, the covering factor and the blackbody contribution, particularly at low luminosities where we have very few objects. For example, it is likely that either the covering fraction and/or the absorbing column vary with luminosity (i.e., low luminosity objects are expected to be more absorbed), although we cannot detect such effect at a significant level in the sample discussed in Section 2. A simple model with constant covering factor and absorbing column is already able to produce very close agreement between the AGN luminosity functions in the soft and hard bands, but it would require some refinement when the data samples can be enlarged.

4 DISCUSSION

We have studied the hardness ratios for a sample of hard X-ray selected sources, all of them observed by ROSAT,

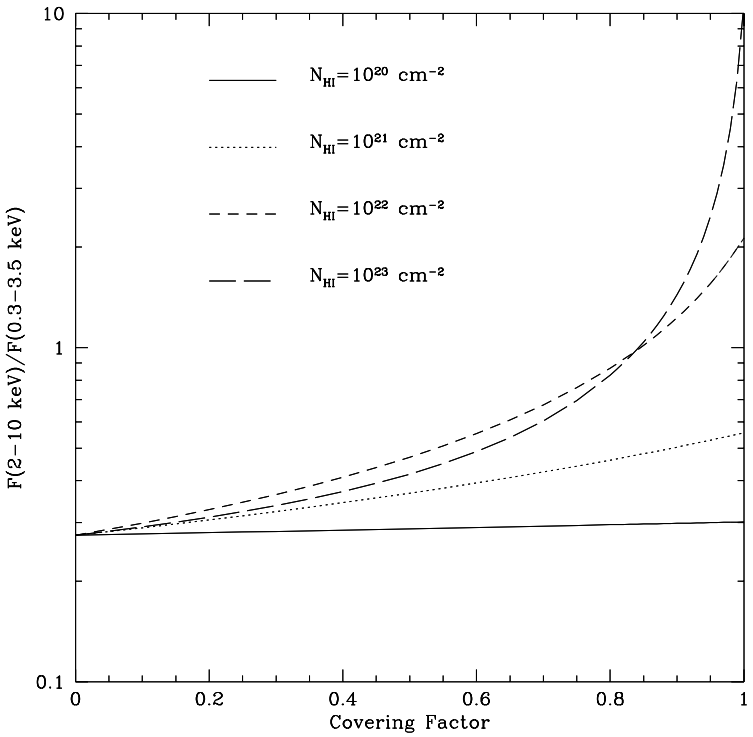

Figure 5. Soft (0.3-3.5 keV) to hard (2-10 keV) X–ray flux ratio versus covering factor. A spectral model with a power law ($\alpha = 0.9$), a blackbody emission ($kT = 0.1$ keV, 50% of the power law at 1 keV) both partially absorbed by different column densities is assumed to draw the lines (solid line for $N_H = 10^{20}\,\mathrm{cm}^{-2}$, dotted line for $N_H = 10^{21}\,\mathrm{cm}^{-2}$, short-dashed line for $N_H = 10^{22}\,\mathrm{cm}^{-2}$ and long-dashed line for $N_H = 10^{23}\,\mathrm{cm}^{-2}$.

and derived a source emission spectrum that would explain their X–ray colours. This spectrum has three components: a power law with an energy index $\alpha \sim 0.9$, a blackbody of $kT \sim 0.1$ keV representing about 50% of the power law at 1 keV and a low-energy absorption by neutral gas with column density $N_H \sim 10^{22} - 10^{23}\,\mathrm{cm}^{-2}$ that partially covers the source ($f_{cov} \sim 80 - 100\%$). Type 2 AGN appear to be fully covered with large column densities while type 1 AGN have an average covering factor ~ 0.82 and absorbing column density $\approx 10^{22}\,\mathrm{cm}^{-2}$. Qualitatively this model can account for the scatter observed in the hardness ratios as well as for the soft excess found in some sources.

A complementary result of our analysis is that starting from a single population of AGN with a distribution of covering factors, it is possible to describe the two distinct populations proposed by Franceschini et al (1993). Their soft X–ray class of active galaxies, showing steep power law spectra and being easily detected by soft X-ray band missions would correspond to those sources that in our model had lower covering factors and eventually exhibit soft excess emission. The hard population would be composed of those sources strongly self-absorbed by high covering factors. The selection of objects in the 2-10 keV band does not particularly favour high values of the covering factor, as it is demonstrated by the presence of a large fraction of partially covered type 1 AGN in the sample used in Section 2. However, for a soft X-ray selected sample, the average covering factor will certainly be smaller. Our model is more alike the one used by Comastri et al (1995) where a single AGN population is used to reproduce the spectrum of the X-ray background.

As far as the mismatch between the number counts in different X-ray bands is concerned, a typical spectrum with a 50% blackbody contribution at 1 keV, a power law energy index $\alpha \sim 0.9$, an absorbing column density between $N_H \sim 10^{22}$ and $N_H \sim 10^{23}$ and a covering factor $f \gtrsim 85\%$ would result in a flux ratio $F(2 - 10\,\mathrm{keV})/\mathrm{F}(0.3 - 3.5\,\mathrm{keV}) \sim 2$ (see Figure 5) which is the required value to solve the discrepancy. Thus, the model presented here with the average parameters obtained in Section 2 also brings the soft and hard source counts into agreement.

We also tried to describe the dispersion on the X–ray colours through a warm absorber model and the conclusion we can extract from this analysis is that the presence of gas in two phases (neutral and partly ionized) is required to reproduce the X–ray colours of most of the sampled AGN.

Finally, we can derive an interesting conclusion from this analysis: the gas responsible for the absorption of the X–ray primary spectrum emitted by the active nucleus must have structure. This structure could be due to holes or to the coexistence of gas in two phases (neutral and ionized).

This research has made use of data obtained through the High Energy Astrophysics Science Archive Research Center Online Service, provided by the NASA-Goddard Space Flight Center. We acknowledge J.P.D. Mittaz and F.J. Carrera at Mullard Space Science Laboratory for help

and Ruth Carballo for careful reading. We also thank the referee for helpful comments and A. Fabian for interesting suggestions. Partial financial support for this research was provided by the Spanish DGICYT under project PB92-0501. MTC was supported by a fellowship from the Universidad de Cantabria.

REFERENCES

Antonucci,R., 1993, ARA&A, 31, 473
Antonucci, R.R.J., Miller, J.S. 1985, ApJ, 297, 621
Avni, Y., Bachall, J.N., 1980, ApJ, 235, 694
Awaki, H., 1992 in Tanaka Y., Koyama K., eds, Frontiers in X-ray Astronomy. Univ. Acad. Press, Tokyo, p.537
Barcons, X., 1993, Adv. Space Res., 13, 253
Boyle, B.J., Shanks, T., Georgantopoulos, I., Stewart, G.C., Griffiths, R.E., 1994, MNRAS, 271, 639
Comastri, A., Setti, G., Zamorani, G., Hasinger, G., 1995, A&A 296, 1
Franceschini, A., Martín-Mirones, J.M., Danese, L., De Zotti, G., 1993, MNRAS, 264, 35
George, I.M. et al 1995, preprint
Gioia, I.M. et al., 1990, ApJS, 72, 567
Giommi,P., Barr, P., Tagliaferri, G., Beuermann, K., Schwope, A., 1989, MNRAS, 236, 375
Grossan, B.A., 1992, PhD thesis, Univ. California at Berkeley.
Hasinger, G., 1992, in Brinkmann W., Trümper J., eds, X-ray emission from Active Galaxies Nuclei and the Cosmic X-ray Background, MPE Report 235, Garching, p.321
Kaastra, J.S., Kunieda, H., Awaki, H., 1991, A&A, 242, 27
Kallman,T.R., McCray, R.A., 1982, ApJS, 50, 263
Kallman,T.R., Krolik, J.H., 1993, NASA Internal Rep.
Kim, D.W., Fabbiano, G., Trinchieri, G., 1992, ApJS, 80, 645
Krolik, J.H., Kriss, G.A., 1995 ApJ, 447, 512
Krolik, J.H., Kriss, G.A., 1996 ApJ, 456, 909
Maccacaro, T., Gioia, I.M., Wolter, A., Zamorani, G., Stocke, J.T., 1988, ApJ, 326, 680
Maccacaro, T., Della Ceca, R., Gioia, I.M., Morris, S.L., Stocke, J.T., Wolter, A., 1991, ApJ, 374, 117
Madau, P., Ghisellini, G., Fabian, A.C., 1994, MNRAS, 270, L17
Marshall, H.L., Avni, Y., Tananbaum, H., Zamorani, G., 1983, ApJ, 269, 35
Matsuoka, M., 1994, in Makino F., Ohashi T., eds., New Horizon of X–ray Astronomy. Univ. Acad. Press, Tokyo, p.305
Murray, N., Chiang, J., 1995, ApJ, 454, L105
Nandra, K., Pounds, K.A., 1994, MNRAS, 268, 405
Netzer, H. 1993, ApJ, 411, 594
Piccinoti, G. et al., 1982, ApJ, 253, 485
Reynolds, C.S., Fabian, A.C., 1995, MNRAS, 273, 1167
Stewart, G.C., 1992, in Barcons X. and Fabian A.C. eds, The X-ray Background. Cambridge University Press, p.259
Tagliaferri, G., Giommi, P., Angelini, L., Osborne, J.P., Pallavacini, R., 1988, ApJ, 331, L113
Turner, T.J., Pounds, K.A., 1989, MNRAS, 240, 833
Turner, T.J., Weaver, K.A., Mushotzky, R.F., Holt, S.S., Madejski, G.M., 1991, ApJ, 381, 85
Turner, T.J. and the BBXRT Science Team, 1992a, in Tanaka Y., Koyama, K., eds, Frontiers in X-ray Astronomy. Univ. Acad. Press, Tokyo, p.541
Turner, M.J.L. et al. 1992b, in Tanaka Y., Koyama K., eds, Frontiers in X-ray Astronomy. Univ. Acad. Press, Tokyo, p.553
Warwick, R.S. and Butcher, J.A., 1992, in Tanaka Y., Koyama K., eds, Frontiers in X-ray Astronomy. Univ. Acad. Press, Tokyo, p.641
Wood, K.S., et al., 1984, ApJS, vol.56, 507

Table 1. The sample

Name	redshift	HR[a]	$F_x(0.5-2)$[b]	$F_x(2-10)$[c]	Type[d]	Ref[e]
3C273	0.1580	0.089±0.010	5.7065±0.047	6.5356±0.559	1	LMA
3C390.3	0.0570	0.824±0.020	0.7459±0.029	1.8257±0.152	1	LMA
AKN374	0.0640	-0.103±0.015	0.5557±0.010	2.4291±0.405	1	LMA
ES0-141-G55	0.0370	0.637±0.012	2.0457±0.032	2.6798±0.251	1	LMA
Fairall9	0.0450	0.172±0.010	2.5278±0.027	3.6052±0.405	1	LMA
H0439-272	0.0800	0.204±0.028	0.4865±0.015	2.5834±0.405	1	LMA
H1029-140	0.0860	0.635±0.007	1.9795±0.020	2.0243±0.347	1	LMA
H1318+692	0.0680	0.062±0.066	0.1298±0.010	1.9857±0.308	1	LMA
H1320+551	0.0640	0.054±0.041	0.1971±0.009	2.0821±0.405	1	LMA
H1419+480	0.0720	-0.064±0.053	0.2569±0.016	2.5834±0.347	1	LMA
IC4329A	0.0160	0.986±0.001	2.8368±0.028	6.3813±0.617	1	LMA
MCG-2-58-22	0.0470	0.367±0.013	3.1853±0.047	3.0846±0.347	1	LMA
MCG-6-30-15	0.0080	0.650±0.009	1.8857±0.024	4.3185±0.559	1	LMA
MKN279	0.0310	-0.079±0.008	2.3228±0.024	3.0846±0.212	1	LMA
MKN290	0.0290	0.190±0.030	0.5307±0.018	2.1207±0.251	1	LMA
MKN352	0.0150	0.877±0.033	0.0997±0.008	2.7954±0.347	1	LMA
MKN376	0.0560	0.875±0.113	0.0131±0.003	3.6052±0.405	1	LMA
MKN464	0.0510	0.393±0.053	0.2469±0.015	3.2967±0.463	1	LMA
MKN478	0.0790	-0.642±0.024	0.7603±0.047	1.8701±0.559	1	LMA
MKN506	0.0430	0.447±0.053	0.3304±0.020	1.8257±0.193	1	LMA
MKN509	0.0350	0.404±0.012	3.8240±0.053	5.3210±0.617	1	LMA
MKN705	0.0280	0.344±0.022	1.0015±0.025	1.9279±0.308	1	LMA
MKN876	0.1290	0.132±0.022	0.4392±0.011	1.9279±0.251	1	LMA
MKN1152	0.0520	-0.018±0.023	0.9415±0.026	3.0846±0.347	1	LMA
MR2251-178	0.0680	0.141±0.016	2.0315±0.037	2.7954±0.617	1	LMA
NGC985	0.0430	0.150±0.019	0.8286±0.018	1.8257±0.308	1	LMA
NGC2992	0.0070	1.000±0.000	0.0853±0.016	4.9740±0.405	2	LMA
NGC3227	0.0030	0.899±0.007	0.4239±0.007	4.4149±0.501	1	LMA
NGC3783	0.0090	0.865±0.013	1.3855±0.040	3.2389±0.463	1	LMA
NGC4151	0.0030	0.206±0.012	0.3234±0.004	4.0100±0.463	1	LMA
NGC4593	0.0090	0.220±0.040	0.9621±0.042	4.2606±0.655	1	LMA
NGC5033	0.0030	0.354±0.044	0.1768±0.009	3.3931±0.868	2	LMA
NGC5506	0.0070	0.957±0.012	0.2373±0.010	1.8701±0.251	2	LMA
NGC5548	0.0170	-0.154±0.008	3.3307±0.034	6.4392±0.405	1	LMA
NGC7172	0.0080	0.355±0.273	0.0056±0.002	1.8701±0.405	2	LMA
NGC7213	0.0060	0.129±0.009	3.5311±0.035	3.2967±0.463	1	LMA
NGC7469	0.0170	0.811±0.005	1.5661±0.015	4.9740±0.501	1	LMA
NGC7582	0.0050	0.725±0.061	0.0370±0.003	4.7619±0.405	2	LMA
NGC7674	0.0290	0.467±0.181	0.0146±0.003	2.5448±0.559	2	LMA
PG0052+251	0.1540	0.478±0.022	0.5366±0.014	4.0100±0.713	1	LMA
PG0804+76	0.1000	0.265±0.025	0.8677±0.024	2.1207±0.308	1	LMA
PictorA	0.0340	0.500±0.335	0.0035±0.001	2.3327±0.308	1	LMA

Table 2. *

Name	redshift	HR[a]	$F_x(0.5-2)^b$	$F_x(2-10)^c$	Type[d]	Ref[e]
3C120	0.0330	0.974±0.005	2.8433±0.069	4.3000±0.430	1	EXO
MKN590	0.0270	0.145±0.013	3.2585±0.047	2.7000±0.270	1	EXO
NGC1068	0.0030	0.120±0.037	1.1321±0.047	0.5300±0.050	2	EXO
NGC6814	0.0050	0.965±0.005	0.2315±0.005	3.0000±0.300	1	EXO
3C111	0.0480	0.991±0.009	0.6151±0.049	3.1300±0.190	1	GINGA
AKN120	0.0330	0.925±0.005	1.8001±0.024	3.5800±0.190	1	GINGA
IIZw136	0.0630	0.205±0.017	0.8046±0.015	0.4800±0.000	1	GINGA
MCG-5-23-16	0.0080	0.957±0.011	0.3378±0.014	2.2400±0.180	2	GINGA
MKN3	0.0137	0.928±0.016	0.0797±0.004	0.8800±0.000	2	GINGA
MKN205	0.0710	0.350±0.025	0.5764±0.016	0.9000±0.000	1	GINGA
MKN335	0.0250	0.015±0.009	1.6386±0.016	1.2500±0.150	1	GINGA
MKN348	0.0150	0.813±0.060	0.0094±0.001	1.1000±0.000	2	GINGA
MKN372	0.0310	0.903±0.010	0.3270±0.009	0.2000±0.000	2	GINGA
MKN841	0.0360	0.020±0.021	1.5708±0.038	0.7900±0.160	1	GINGA
NGC1808	0.0030	0.925±0.020	0.0636±0.004	0.3000±0.000	2	GINGA
NGC3516	0.0090	0.305±0.007	3.4997±0.025	2.0900±0.190	1	GINGA
NGC4051	0.0020	-0.247±0.026	0.3700±0.013	1.9500±0.170	1	GINGA
NGC7314	0.0060	0.969±0.004	0.2243±0.004	2.8300±0.180	2	GINGA
PG1211+143	0.0850	-0.162±0.031	0.6110±0.024	0.7700±0.000	1	GINGA
PG1307+085	0.1550	-0.048±0.029	0.2487±0.009	0.6400±0.000	1	GINGA
PG1352+183	0.1520	-0.268±0.025	0.2087±0.007	0.1600±0.000	1	GINGA
PG1416-129	0.1290	0.879±0.012	0.4032±0.011	0.6600±0.000	1	GINGA
PHL1657	0.2000	0.498±0.054	0.3366±0.022	1.1800±0.000	1	GINGA

(continued)

[a] Hardness Ratio not corrected for Galactic absorption
[b] Flux in $10^{-11}\mathrm{erg\,cm^{-2}\,s^{-1}}$ in the (0.5-2) keV band
[c] Flux in $10^{-11}\mathrm{erg\,cm^{-2}\,s^{-1}}$ in the (2-10) keV band
[d] Type: 1 for Sy1/QSO and 2 for Sy2
[e] References for 2-10 keV Flux: LMA (Grossan 1992), EXO (Turner & Pounds 1989), GINGA (Nandra & Pounds 1994, Turner et al 1992b, Awaki 1992)